

# Molecular Determinants for the Layering and Coarsening of Biological Condensates

Andrew Latham<sup>1</sup> and Bin Zhang<sup>1</sup>

<sup>1</sup>MIT

November 8, 2022

## Abstract

Many membraneless organelles, or biological condensates, that play key roles in signal sensing and transcriptional regulation form through phase separation. While the functional importance of these condensates has inspired many studies to characterize their stability and spatial organization, the underlying principles that dictate these emergent properties are still being uncovered. In this review, we examine recent work on biological condensates, especially multicomponent systems. We focus on connecting molecular factors such as binding energy, valency, and stoichiometry with the interfacial tension, explaining the nontrivial interior organization in many condensates. We further discuss mechanisms that arrest condensate coalescence by lowering the surface tension or introducing kinetic barriers to stabilize the multidroplet state.

# Molecular Determinants for the Layering and Coarsening of Biological Condensates

Andrew P. Latham<sup>1,2</sup> | Bin Zhang\*<sup>1</sup>

<sup>1</sup>Department of Chemistry,  
Massachusetts Institute of  
Technology, Cambridge, MA 02139

<sup>2</sup>Department of Bioengineering and  
Therapeutic Sciences, University of  
California at San Francisco, San  
Francisco, CA 94143

## Correspondence

\*Bin Zhang. Email: binz@mit.edu

## Abstract

Many membraneless organelles, or biological condensates, that play key roles in signal sensing and transcriptional regulation form through phase separation. While the functional importance of these condensates has inspired many studies to characterize their stability and spatial organization, the underlying principles that dictate these emergent properties are still being uncovered. In this review, we examine recent work on biological condensates, especially multicomponent systems. We focus on connecting molecular factors such as binding energy, valency, and stoichiometry with the interfacial tension, explaining the nontrivial interior organization in many condensates. We further discuss mechanisms that arrest condensate coalescence by lowering the surface tension or introducing kinetic barriers to stabilize the multidroplet state.

## KEYWORDS

membraneless organelle, biological condensate, phase separation, intrinsically disordered protein, surface tension

## INTRODUCTION

Cells constantly perform myriads biochemical reactions in parallel. To avoid crosstalks and interference among different pathways, cells compartmentalize into membrane-bound vesicles that enclose specific sets of molecules. The recently discovered membraneless organelles, also known as biological condensates, could offer similar specificity by concentrating functionally related molecules via self-assembly, providing additional levels of structure and organization within the cell.<sup>[1–5]</sup> Many biological condensates are dynamic and exhibit liquid-like properties. They allow fast molecular

exchange with the cellular environment and can assemble/dissolve on demand in response to external signals that modulate the concentration and chemical state of its components.<sup>[6–8]</sup>

Biological condensates are involved in a variety of processes throughout the cell. For instance, stress granules form in the cytosol as a mechanism of cellular stress response to protect RNAs from harmful chemicals.<sup>[9]</sup> TIS granules form at the interface with the endoplasmic reticulum to assist in the translation of mRNA and the formation of membrane protein complexes.<sup>[10,11]</sup> Inside the nucleus, membraneless organelles contribute to genome organization, partitioning chromosomes into active and silent domains.<sup>[1–3,12]</sup> They may assist DNA compaction in heterochromatin<sup>[13,14]</sup> or promote transcription as in the case of condensates formed by super-enhancers.<sup>[15]</sup>

Significant progress has been made in understanding the mechanisms of biomolecular condensate formation *in vitro*. In particular, intrinsically disordered proteins (IDPs) are found in many membraneless organelles. They undergo phase separation at cellular concentrations to form dynamic droplets.<sup>[16–19]</sup> The propensity of IDPs to phase separate arises mainly from their ability to associate simultaneously with multiple partners, i.e., high valency. IDPs often harbor several disordered segments that promote electrostatic, cation- $\pi$ ,  $\pi$ - $\pi$ , hydrogen bonding, or hydrophobic interactions.<sup>[20]</sup> In the meantime, specific interactions between ordered regions with well-defined protein-protein interfaces can also contribute to the multivalency.<sup>[21–23]</sup> Finally, nucleic acids can also form condensates.<sup>[24,25]</sup> Similar to motifs in proteins, multivalent interactions between nucleic acids contribute to their phase separation propensity.<sup>[26,27]</sup>

While the mechanisms of single-component systems are well understood, biological condensates in the cell contain many components, including proteins, DNA, and RNA. The complex molecular composition of these condensates gives rise to more elaborate mechanisms. For instance, higher valency proteins, frequently referred to as scaffolds, can drive the formation of condensates and incorporate lower valency proteins that are not capable of phase separation on their own, which are often called clients.<sup>[21,32,33]</sup> Additionally, many biomolecules are highly charged, and Coulombic interactions can drive their condensation through a mechanism known as complex coacervation.<sup>[34,35]</sup> Complex coacervates exemplify a broader class of condensates stabilized by cross-interactions between components. In such cases, condensate stability is often dependent on stoichiometry, resulting in reentrant phase separation.<sup>[36,37]</sup> Bridging-induced polymer collapse has been proposed as a mechanism to explain the formation of chromatin bodies.<sup>[38,39]</sup> For example, protein molecules may bind with chromatin in multiple locations to introduce physical crosslinks or bridges, the accumulation which induces polymer collapse to form condensates. For more information on the mechanisms of biomolecular phase separation, we refer the reader to several of many great existing reviews.<sup>[17–20,40]</sup>

The complexity in molecular composition also produces novel condensate internal organizations and coarsening behaviors deviating from homogeneous mixtures.<sup>[20,41,42]</sup> Order-disorder transitions could occur to form substructures via microphase separation as in block-copolymer systems, producing layering in the condensates.<sup>[43,44]</sup>

The presence of substructures may facilitate the mini-factories to further streamline the processing and synthesis of biomolecules with dedicated platforms by division of labor. Novel behaviors in phase separation kinetics have also been observed in biological condensates. Defying expectations from the classical nucleation theory, condensates inside cells are often arrested in a multi-droplet state.<sup>[45]</sup> Further coarsening is rarely observed over timescales spanning the entire cell cycle ( $\sim 24$  hours).<sup>[46]</sup>

In this review, we examine molecular mechanisms giving rise to emergent behaviors of biological condensates. We begin by exploring examples of condensates with non-trivial internal organizations. Next, we argue that the sub-structures in condensates can be understood and predicted from the interfacial tension among immiscible liquids. Further connecting molecular interactions with interfacial tension provides a conceptual framework to interpret various experimental observations on condensate stability and organization. We conclude the review by examining the physical characteristics that prevent droplet fusion and thus limit the size of biomolecular condensates.

## LAYERED INTERNAL ORGANIZATION OF BIOLOGICAL CONDENSATES

Many biological condensates display substructures to provide additional spatial and physical control necessary for complex functions. The nucleolus, essential for ribosome biogenesis, presents an excellent example highlighting the advantages of a layered interior organization.<sup>[47,48]</sup> It is composed of three layers, the fibrillar center, the dense fibrillar component, and the granular component. This organization allows for each part of the nucleolus to have different protein compositions and perform distinct biological functions: rDNA is transcribed in the fibrillar center, the resulting rRNA is processed in the dense fibrillar center, and ribosome assembly occurs in the granular component (Figure 1A).<sup>[28,49]</sup> Such a division of labor helps streamline ribosome production and assembly by assigning steps to different regions of the nucleolus.

The nuclear speckle is another example that displays a layered organization, and the functional significance of maintaining such intricate internal structures is only beginning to emerge. Nuclear speckles are composed of both RNA and protein components and are essential for gene transcription and splicing.<sup>[50]</sup> Recent studies have shown that many RNA components, including snRNA

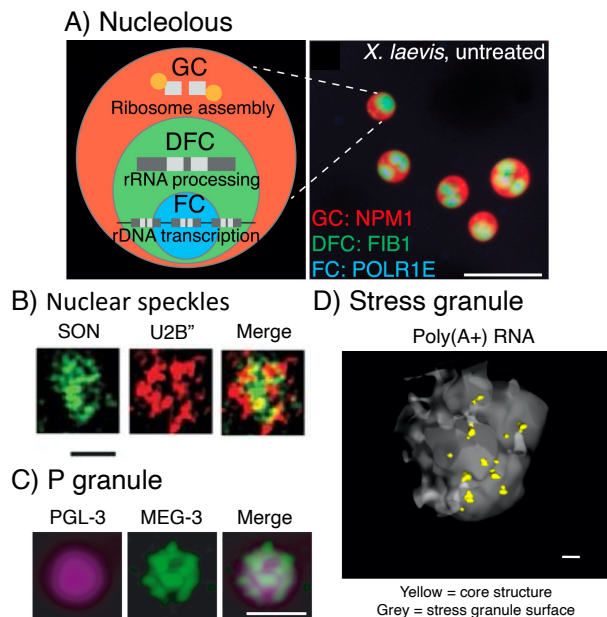


**FIGURE 1** Examples of biological condensates with a layered organization. A, left) Schematic diagram of subcompartments within the nucleolus. A, right) Nucleoli within an untreated *X. laevis* nucleus. NPM1 (red), FIB1 (green) and POLR1E (blue) are tagged. Scale bar, 20  $\mu\text{m}$ . Image modified from<sup>[28]</sup> with permission from Elsevier. B) Organization of two components within nuclear speckles, the protein SON and the snRNA U2B''. Scale bar, 1  $\mu\text{m}$ . Adapted with permission from the Journal of Cell Science.<sup>[29]</sup> C) Photomicrographs examining the *in vivo* assembly of MEG-3:mEGFP and PGL-3:mCherry, two main components of P granules. Scale bar, 500 nm. Image minimally modified from.<sup>[30]</sup> Reprinted with permission from AAAS. D) Stochastic optical reconstruction microscopy (STORM) image of a stress granule (gray), highlighting poly(A+) RNA cores (yellow). Scale bar, 500 nm. Image modified from<sup>[31]</sup> with permission from Elsevier.

like U2B'', localize toward the exterior of the condensate, and scaffold proteins, such as SON, localize toward the interior (Figure 1B).<sup>[29,51,52]</sup> This organization may serve as a mechanism to control condensate size, as the accumulation of pre-mRNA at the periphery can recruit more speckle components.<sup>[29]</sup> Further, the localization of RNA to the exterior of the condensate may aid in biological function, for the interface between speckles and the nucleoplasm is likely the location of RNA splicing.<sup>[53]</sup>

In addition to their differences in molecular composition, the various layers could exhibit distinct material properties as well. For example, the two layers in P granules are found to be either liquid-like or gel-like. P granules are the first proposed droplets formed through liquid-liquid phase separation and localize in the posterior half of *C. elegans* embryos.<sup>[54]</sup> The phase separation is driven by the protein, MEG-3,<sup>[55]</sup> which was later shown to form gel-like assemblies closer to the exterior of the P granules (Figure 1C).<sup>[30,56]</sup> Meanwhile, the core of the P-body contains RNA-binding proteins such as PGL-3 and remains liquid-like.

Similar to P granules, stress granules were found to have liquid and gel-like compartments.<sup>[58]</sup> Using stochastic optical reconstruction microscopy (STORM), Jain et

al. demonstrated that stress granules contain core structures consisting of both proteins and mRNA (Figure 1D).<sup>[31]</sup> Later work demonstrated that protein dynamics within these core structures is slower than that within the surrounding medium.<sup>[59]</sup> Time course analysis further showed that these cores form as precursors to the assembly of the liquid shell.<sup>[60]</sup>

Both molecular specificity and differential physical properties could contribute to substrate selectivity among the substructures, as elegantly shown in a recent *in vitro* study. Choi et al. characterized a layered condensate formed by arginine repeats (polyR) and lysine repeats (polyK) with aspartic acid repeats (polyD).<sup>[61]</sup> They observed the layering of polyR dominant and polyK dominant phases and tested the affinity of different phases for nucleic acid substrates, specifically dsRNA and ssRNA. As expected, ssRNA partitioned into the inner, polyR layer. However, dsRNA partitioned into the polyK layer as a result of their increased stiffness and lack of cation- $\pi$  interactions. Finally, its differential preference of ssRNA led to significant dehybridization of RNA duplexes within the polyR condensate layer.

Besides the above examples, other biological condensates, including paraspeckles,<sup>[62]</sup> anisosomes,<sup>[63]</sup> Cajal

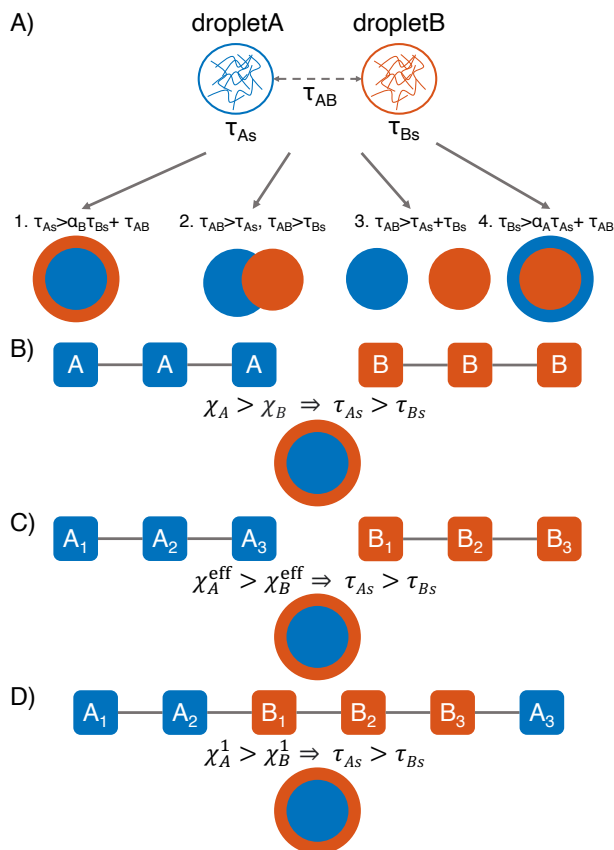


FIGURE 2 Relation between interfacial tension ( $\tau$ ), effective interaction parameter ( $\chi$ ), and condensate organization. A) Mixing two immiscible droplets can lead to four possible organizations: (1) a layered droplet with dropletA on the inside, (2) partially wetted droplets that share an interface (3) complete nonwetting to form two separate droplets, and (4) a layered droplet with dropletB on the inside. The most stable organization is determined by the interfacial tension between dropletA and dropletB ( $\tau_{AB}$ ), between dropletA and the solvent phase ( $\tau_{As}$ ), and between dropletB and the solvent phase ( $\tau_{Bs}$ ). The droplet size ( $\alpha_A$  and  $\alpha_B$ ) can also contribute to the condensate organization, as demonstrated by Lu and Spruijt.<sup>[57]</sup> B) For immiscible homopolymers, the Flory-Huggins interaction parameter ( $\chi_A$ ,  $\chi_B$ ) can provide a way to approximate differences in surface tension. C) Flory-Huggins theory can be generalized to heteropolymers by assuming an effective interaction parameter that averages over differences in the sequence ( $\chi_A^{\text{eff}}$ ,  $\chi_B^{\text{eff}}$ ). D) Heteropolymers can be divided into segments with different physical properties, resulting in effective parameters for different portions of the single chain ( $\chi_A^1$ ,  $\chi_B^1$ ).

bodies,<sup>[64,65]</sup> and mitochondrial transcriptional condensates,<sup>[66,67]</sup> have been known to display complex organization as well. While the physical and biological implications of these structures have been discussed and remain of interest for future studies,<sup>[41,46,49,68]</sup> how these organizations emerge from molecular level descriptions of the system has not been adequately reviewed. In the next section, we focus on the physical principles that dictate the internal organization of biological condensates, with a particular emphasis on connecting interactions among components to macroscopic condensate behaviors.

## MOLECULAR DETERMINANTS OF CONDENSATE ORGANIZATION

Insights into the internal organization of biological condensates can be gained from studies of immiscible liquids. In particular, the geometric outcome for mixing two immiscible droplets is predictable with thermodynamic arguments in terms of their relative surface tensions.<sup>[28,41,49,57,68,69]</sup> Two immiscible droplets (dropletA and dropletB) can form four unique configurations (Figure 2A): a layered organization with dropletA on the inside, a layered organization with dropletB on the inside, complete nonwetting to form two separate droplets, and partial wetting into two droplets that share an interface. Therefore, interfacial tensions provide a complete phenomenological description of condensate organization. However, they are emergent properties, and connecting

interfacial tensions with the molecular composition is nontrivial.

Microscopic theories help connect surface tension with molecular interactions. The Flory-Huggins theory based on lattice models has proven successful at understanding the thermodynamics of polymer phase separation.<sup>[70]</sup> An essential parameter in the theory is

$$\chi = \frac{z}{2k_B T} [\epsilon_{pp} + \epsilon_{ss} - \epsilon_{ps}] = \frac{z\Delta\epsilon}{2k_B T}, \quad (1)$$

which accounts for the preferences of homotypic interactions, namely polymer-polymer ( $\epsilon_{pp}$ ) and solvent-solvent ( $\epsilon_{ss}$ ), over heterotypic solvent-polymer interactions ( $\epsilon_{ps}$ ). The coordination number ( $z$ ), temperature ( $T$ ), and Boltzmann constant ( $k_B$ ) also determine  $\chi$ . The theory correctly predicts the dependence of the critical temperature for phase separation on the interaction strength and length of polymers. Generalization of the theory that accounts for both enthalpic and entropic contributions to  $\chi$  explains the presence of upper liquid critical temperature for certain polymers. Furthermore, it has been shown that the interfacial tension is directly related to  $\chi^\alpha$ .<sup>[71,72]</sup> While the exact value of the exponent,  $\alpha$  is subject to debate, a positive correlation between the two is clear. Therefore, increasing the propensity for homotypic polymer interactions over heterotypic polymer interactions will also increase the surface tension between the polymer and solution phases (Figure 2B).

The above arguments provide a powerful conceptual framework for interpreting experimental observations. For example, poly(proline-arginine) is known to form layered droplets with RNA, where poly-C RNA localized at the solvent interface and poly-A RNA comprised the core.<sup>[73]</sup> Modeling demonstrated that this result may occur due to a stronger affinity of poly(proline-arginine) for poly-A RNA than poly-C RNA, a stronger self-affinity of poly-A relative to poly-C, or less favorable interactions for poly-A. Each of these interaction schemes will produce higher  $\chi$  values and surface tension for the droplet formed by poly-A than those formed by poly-C. Similar results were seen when studying mixtures of arginine repeats (polyR) and lysine repeats (polyK) with uridine-5'-triphosphate trisodium salt (UTP), where polyR formed a core and polyK formed a shell. The differences between the layers were attributed to stronger R-UTP interactions than K-UTP interactions due to the ability to form pi-pi interactions (Figure 3A-C). These stronger interactions with polyR explain the higher surface tension of the corresponding droplet.<sup>[74]</sup> Elastin-like polypeptides are another model IDP system that supports similar behaviors. More hydrophobic sequences

have higher values of  $\chi$  and populate at the condensate interior.<sup>[75]</sup>

While the Flory-Huggins theory was derived for homopolymers, it can be applied to heteropolymers and complex systems by averaging polymer-polymer and polymer-solvent interactions over the sequence to produce an effective  $\chi$  (Figure 2C). For example, polymers with more solvated linkers will, on average, have smaller  $\chi$  values and be pushed to the shell of the droplet, while linkers with less solvation volume will localize toward the interior.<sup>[78]</sup> Higher valency has been seen to correlate with the interior of the condensate, as a result of stronger effective interactions.<sup>[79]</sup> In a recent study, Latham and Zhang simulated the phase separation of a mixture of two chromatin regulators, HP1 $\alpha$  and histone H1, with DNA with the MOFF force field.<sup>[80–83]</sup> They observed that H1 localizes toward the droplet-solvent interface and HP1 $\alpha$  is located toward the middle of the droplet. The observed layering can be explained by stronger HP1 $\alpha$ -HP1 $\alpha$  interactions relative to H1-H1 interactions (Figure 3D-E).<sup>[76]</sup>

The effective  $\chi$  value depends not only on the chemical composition of the molecule but also on the precise arrangement of the chemical groups. In a computational study, Regy et al. shuffled the sequence of the RGG domain of LAF1 and explored its phase behavior with RNA, specifically a 15 nucleotide adenosine repeat (A<sub>15</sub>).<sup>[77]</sup> They found that a shuffled sequence with more charge blockiness (RGG<sub>Cshuf</sub>) led to stronger protein-protein and protein-RNA interactions. Further, the minimum of the protein-RNA potential of mean force moved such that it is minimized when the two biomolecules are held approximately 20Å apart instead of at a mean distance of zero (Figure 3F). Because of these changes, RGG<sub>Cshuf</sub> and RNA formed a layered condensate, with RNA located on the exterior of the condensate (Figure 3G,H). Other computational work on polyampholytes has found similar results. Using sequence-specific modeling of K/E mixtures of the same overall composition, Pal et al. showed that differences in the blockiness of charge distribution can drive condensate layering, likely through changes to the shape or depth of the pairwise PMF for the two chains.<sup>[84]</sup>

The effective averaging procedure is inherently a mean-field assumption, which breaks down when functional groups with strong interactions stick together to form clusters. Clustering and even microphase separation can lead to layered organizations in single component systems as well, as seen in condensates formed with the Velo1 N-terminal prion-like domain.<sup>[85]</sup> The association of aromatic residues slows down protein dynamics and

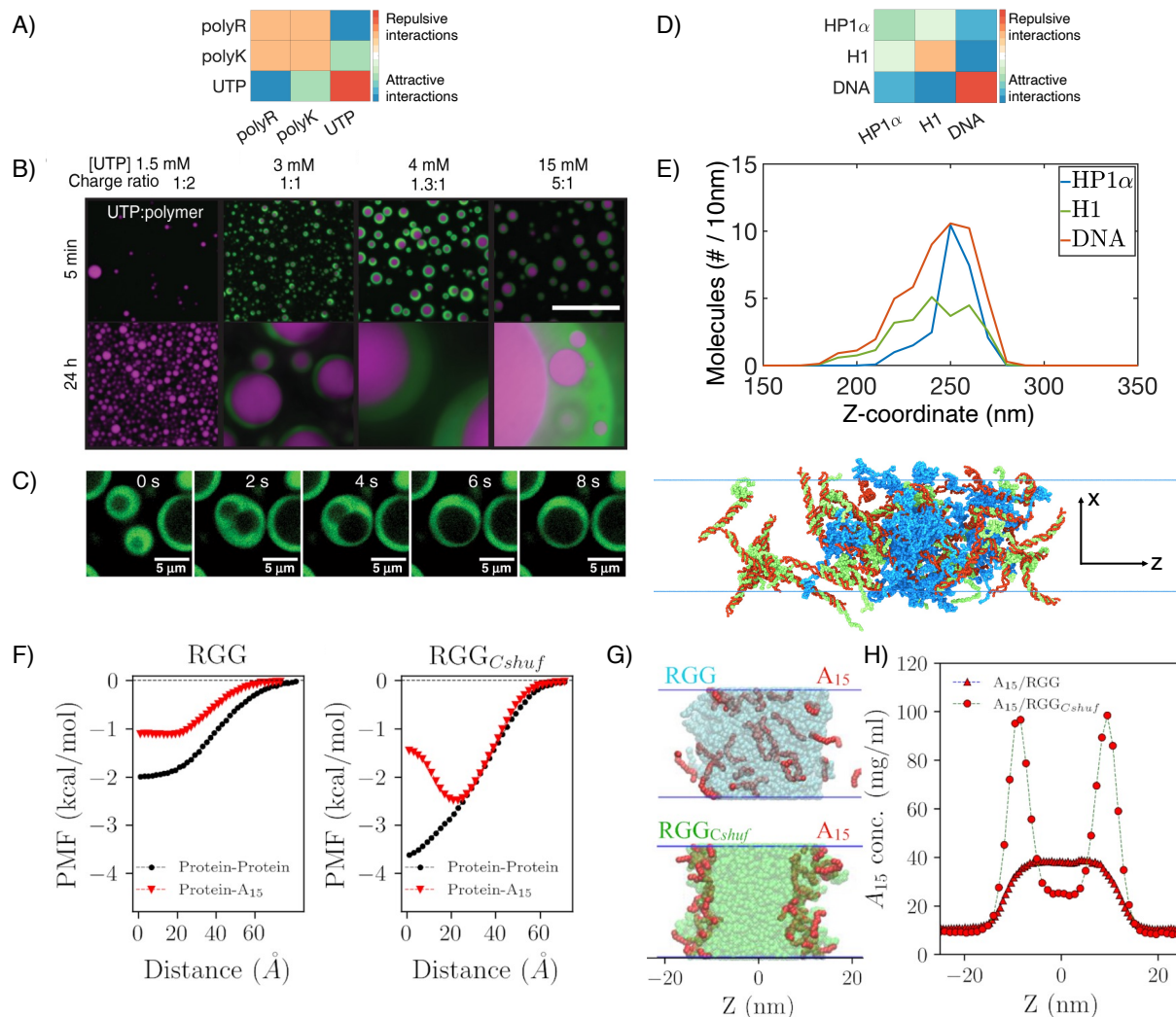


FIGURE 3 Molecular factors that drive the formation of layered condensates. (A) Hypothetical interaction patterns of polyR, polyK, and UTP that explain the observed condensate organization. (B) Confocal fluorescence images of 50:50 polyK(green):polyR(purple) mixtures at different ratios of UTP. Scale bar, 20  $\mu\text{m}$ . (C) Confocal fluorescence images of fusion of layered coacervates. polyK is labeled in green, and polyR is unlabeled. Images modified from ref.<sup>[74]</sup> CC BY 4.0. (D) Approximate interaction patterns of HP1 $\alpha$ , H1, and DNA, which also results in a layered condensate. (E) The slab density profiles support a layered organization for mixtures of HP1 $\alpha$  (blue), H1 (green), and DNA (red). HP1 $\alpha$  coalesces toward the center of the droplet, with H1 to the outside. Image modified from<sup>[76]</sup> with permission from Elsevier. (F) Potential of mean force (PMF) for protein-protein and protein-RNA interactions with the native LAF1-RGG sequence (RGG) and the shuffled RGG sequence (RGG<sub>Cshuf</sub>). (G) Simulation snapshots indicating the preference of A<sub>15</sub> to localize to the condensate exterior with RGG<sub>Cshuf</sub> but not RGG. (H) Density profiles of A<sub>15</sub> in RGG and RGG<sub>Cshuf</sub> condensates. Reprinted from<sup>[77]</sup> with permission from Oxford University Press.

renders the corresponding condensate more solid-like. Similar results were seen in a computational work on the RNA binding protein Fused in Sarcoma (FUS).<sup>[86]</sup> The authors modeled a disordered-to-ordered transition in the prion-like domain that is expected upon condensate aging. After the transition, the higher self-affinity among prion-like domains drove a layered organization and their interior localization.<sup>[87]</sup> For these systems, by dividing the molecules into multiple groups with individual effective  $\chi$  values, their organization can be analyzed

similarly to the multi-component systems mentioned above (Figure 2D).

The energetics-focused perspective outlined above may miss certain features of phase separation. For instance, experiments have demonstrated that arginine-rich polypeptides can form layered droplets with RNA, with the component in excess preferentially located on the exterior.<sup>[88]</sup> Modeling has since demonstrated that the polymer in excess localizes to the interface due to the entropic gain of providing multiple binding partners. Further, as the stoichiometry becomes more unbalanced, the

amount of unbound polymer at the interface increases, which decreases the surface tension of the condensate.<sup>[89]</sup> In addition, non-equilibrium processes can also play a role in condensate organization. Using a model of the human genome,<sup>[90,91]</sup> Jiang et al. examined the role of active forces, such as those that arise from transcription or chromatin remodeling,<sup>[92,93]</sup> on phase separation, genome structure, and genome dynamics.<sup>[94]</sup> They found that applying active forces to euchromatin pushes heterochromatin to the nuclear periphery. This organization competes with strong attractive interactions, which pull heterochromatin toward the center of the nucleus. Similar active processes may play a role in the organization of other systems, including transcriptional condensates.<sup>[15]</sup>

## LIMITATIONS ON CONDENSATE COARSENING

While thermodynamic arguments regarding surface tension have proven successful at explaining many experimental results, some observations appear to defy predictions. In particular, a single condensate is expected at equilibrium to minimize the surface energy.<sup>[95,96]</sup> However, multiple nucleoli ( $\sim 2$ -5) can stably coexist in the same nucleus,<sup>[97]</sup> as can paraspeckles<sup>[98]</sup> and nuclear speckles.<sup>[99]</sup> Mechanisms that prevent the coarsening and fusion of biological condensates are only beginning to emerge.

The complexity in the molecular interactions that drive condensate formation and their internal organization may produce micelle-like structures with low surface tension, reducing the driving force for coarsening. Similar to surfactants that harbor both hydrophobic and hydrophilic groups, molecules found in condensates differ in their valency. High valency molecules prefer polymer-polymer over polymer-solvent interactions and are thus more “hydrophobic” than low valency ones. The accumulation of low-valency molecules at the condensate exterior could lower the interfacial tension. To demonstrate this principle, Sanchez-Burgos et al. used a minimal scaffold-surfactant model, where scaffolds and surfactants are particles with high and low valency, respectively. They showed that the surface tension, and hence the number of droplets, was tunable by the surfactant-scaffold ratio (Figure 4A).<sup>[100]</sup> This computational framework has been seen in biological contexts. For example, high valency complexes of G3BP and UBAP2L cause the formation of stress granules, while the low valency of USP10 allows it to act as a cap to inhibit stress granule growth.<sup>[103,104]</sup>

Similar behaviors were also found in a designed Arti-Granule (ArtiG) system.<sup>[101]</sup> Navarro et al. designed *in vivo* RNA-protein assemblies by modifying versions of the human ferritin protein to increase its self-interaction (mCherry-FFm), and further added domains to recruit specific RNA targets (PUM.HD-FFm). They then varied the ratios of mCherry-FFm to PUM.HD-FFm, and observed condensates with more RNA binding elements tended to form smaller condensates than those driven by the self-affinity of FFm alone (Figure 4B). The authors proposed that RNA binding creates steric hindrance to limit the valency of surface FFm molecules, which prevents condensate fusion.

Localization of disordered proteins to the interface of condensates can also control the size of biological condensates through other mechanisms. Recent work on P granules suggests that the disordered protein MEG-3 can act as a Pickering agent.<sup>[105]</sup> Folkmann et al. observed that MEG-3 proteins form low dynamic assemblies resembling solid particles, which coat the surface of P granules to reduce the surface tension.<sup>[30]</sup> Depleting MEG-3 causes P granules to increase dramatically in size.

In addition to lower thermodynamic driving forces, condensate fusion may be slowed down due to kinetic barriers. For example, net charges can induce an accumulation of counterions near the condensate surface, giving rise to the so-called zeta potential. Higher zeta potentials slow or prevent condensate fusion due to stronger electrostatic repulsion.<sup>[106]</sup> Additionally, fusion barriers could arise from breaking existing structures inside the droplets. Using a stickers and spacers model, Ranganathan and Shakhnovich demonstrated that strong interactions with low valency produce finite-sized droplets with saturated interaction sites.<sup>[22]</sup> Existing interactions must be abolished for these droplets to grow. Similarly, TIS granules, which are biological condensates that form near the endoplasmic reticulum,<sup>[10,11]</sup> were found to have mesh-like shapes originating from the underlying network of cross-linked, disordered RNA. Fusion of such condensates would require a breakdown of the mesh that faces an enormous energetic penalty.

Just as the structural organization of condensates can hinder their fusion, structures within the solvent phase can also arrest condensate coalescence. Through explicit simulations of the phase separation process for nucleoli formation with the presence of a chromatin network,<sup>[90,91]</sup> Qi and Zhang showed that the reorganization of chromatin creates an entropic barrier to nucleoli fusion,<sup>[102]</sup> and accounts for the observation that many separate nucleoli are observed in the cell (Figure 4C-E).<sup>[107]</sup> Other studies have also considered

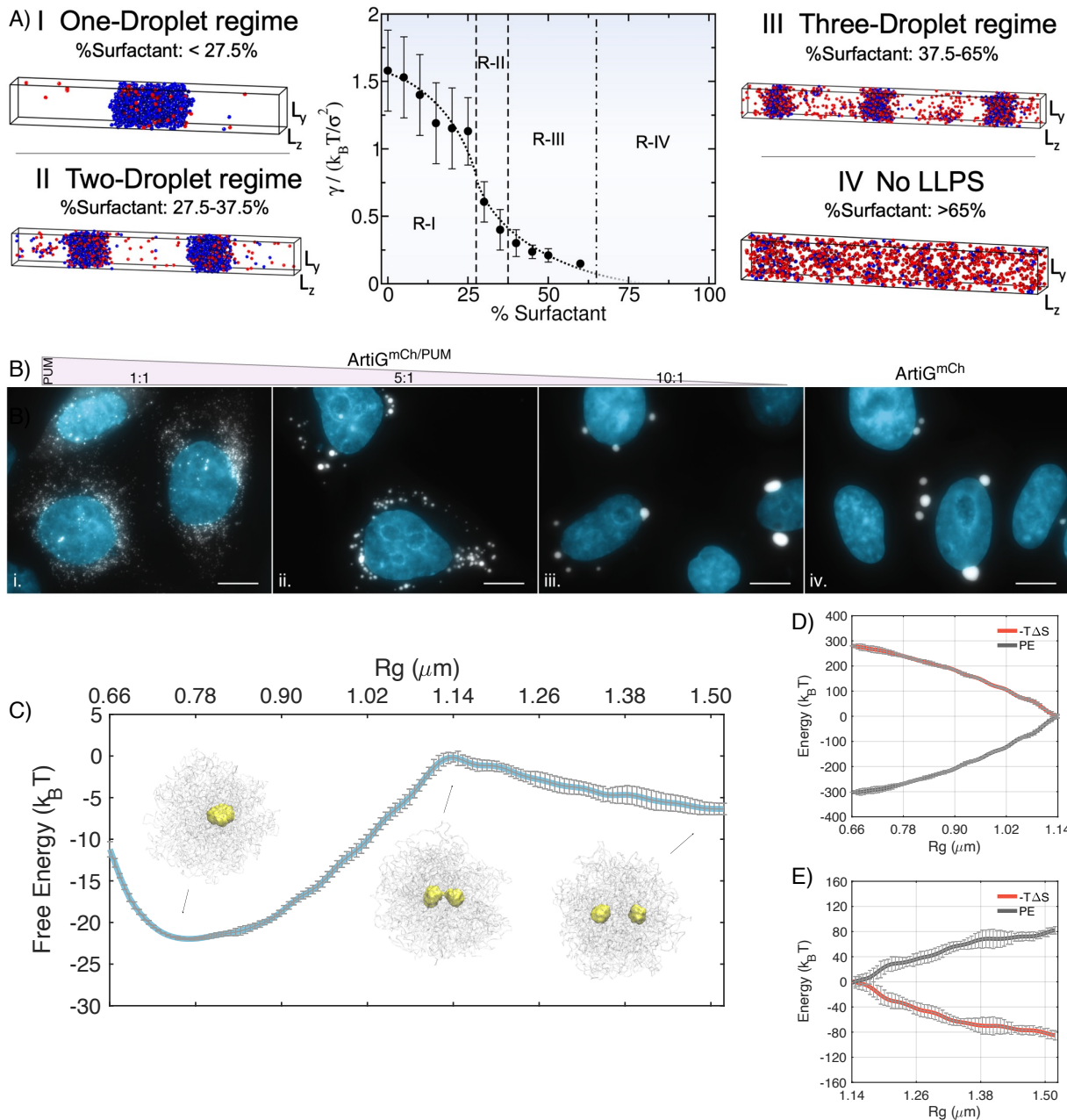


**FIGURE 4** Molecular factors that limit condensate growth. (A) Computational evidence that lower valency surfactants can limit droplet growth. Surface tension ( $\rho$ ) depends on the ratio of surfactants (red) to scaffold (blue). Vertical dashed lines indicate the maximum surfactant concentration that allows for phase separation for a given number-droplet regime. Note that the maximum droplet size varies continuously with surfactant concentration even within the same number-droplet regime. Snapshots of simulations in each droplet regime are included. Images modified from ref.<sup>[100]</sup> CC BY 4.0. (B) RNA binding modifies ArtiG size. Confocal images of ArtiG in HeLa cells, 24 hours after transfection of mCherry-FFm and PUM.HD-FFm constructs at ratios of 1:1 (i), 5:1 (ii), 10:1 (iii), and 1:0 (iv). ArtiG<sup>mCh</sup> indicates ArtiG comprised of mCherry-FFm, while ArtiG<sup>mCh</sup><sup>PUM</sup> indicates ArtiG comprised of both mCherry-FFm and PUM.HD-FFm. Images modified from ref.<sup>[101]</sup> CC BY 4.0. (C) Computational modeling shows the presence of an entropic barrier that stabilizes the two-droplet state for nucleoli. Free energy profile as a function of the radius of gyration, which effectively measures the distance between the two droplets. The free energy is broken into entropic (red) and energetic (black) components before (D) and after (E) the barrier for droplet fusion. Images modified from ref.<sup>[102]</sup> CC BY 4.0.

droplet growth in the nucleus by modeling the nucleus as an elastic network.<sup>[108–111]</sup> In these cases, the mechanical stress of the permanently cross-linked network was

attributed to arresting the coarsening dynamics of condensates. As the dynamical processes of chromatin are known to be timescale dependent,<sup>[112]</sup> both the entropic

barrier of chromatin reorganization and the mechanical stress of disrupting the chromatin network may limit the coarsening of condensates within the nucleus.

Finally, active processes can also contribute to the arrest of condensate coalescence. Wurtz and Lee introduced a theoretical model in which phase-separating molecules can be converted into soluble molecules through chemical reactions. For certain reaction rates, the steady state of the system corresponds to many monodisperse droplets.<sup>[113]</sup> This model may be applicable to a variety of membraneless organelles in the cell, where changes such as post-translational modifications could serve as a control mechanism to inhibit condensate growth.<sup>[114]</sup> To demonstrate the role of active processes in a biological context, Guilhas et al. studied ParABS, a system responsible for chromosome and plasmid segregation in bacteria.<sup>[115]</sup> While the ParB protein drove phase separation, they found that ParA, specifically ParA's ATPase activity, was necessary to control the size and location of ParABS condensates. Similar mechanisms may also play a role in other condensates, including P granules<sup>[116]</sup> and stress granules,<sup>[117,118]</sup> where enzymatic activity has been shown to dissolve condensates.<sup>[114]</sup>

## CONCLUSIONS AND FUTURE OUTLOOK

In this review, we have discussed the molecular factors that dictate the interfacial tension and, thus, the size and structure of biological condensates. Such factors include interaction energy between components, valency, stoichiometry, topological constraints, etc. Continued advances in experimental, computational, and theoretical methods should lead to the discovery of many new biological condensates and improved characterization of existing ones. Such discoveries may allow scientists to perturb and engineer biological condensates for therapeutic purposes.

## ACKNOWLEDGMENTS

This work was supported by the National Institutes of Health (Grant R35GM133580) and the National Science Foundation (Grant MCB-2042362). A.L. further acknowledges support by the National Science Foundation Graduate Research Fellowship Program.

## CONFLICT OF INTEREST

The authors declare no potential conflict of interests.

## REFERENCES

1. B. R. Sabari, A. Dall'Agnese, R. A. Young, *Trends Biochem. Sci.* **2020**, *45*, 961.
2. S. Sanulli, G. J. Narlikar, *Curr. Opin. Cell Biol.* **2020**, *64*, 90.
3. S. F. Banani, H. O. Lee, A. A. Hyman, M. K. Rosen, *Nat. Rev. Mol. Cell Biol.* **2017**, *18*, 285.
4. V. N. Uversky, *Curr. Opin. Struct. Biol.* **2017**, *44*, 18.
5. J. B. Woodruff, A. A. Hyman, E. Boke, *Trends Biochem. Sci.* **2018**, *43*, 81.
6. D. Hnisz, K. Shrinivas, R. A. Young, A. K. Chakraborty, P. A. Sharp, *Cell* **2017**, *169*, 13.
7. J. A. Riback, L. Zhu, M. C. Ferrolino, M. Tolbert, D. M. Mitrea, D. W. Sanders, M. T. Wei, R. W. Kriwacki, C. P. Brangwynne, *Nature* **2020**, *581*, 209.
8. I. A. Klein, A. Boija, L. K. Afeyan, S. W. Hawken, M. Fan, A. Dall'Agnese, O. Oksuz, J. E. Henninger, K. Shrinivas, B. R. Sabari, I. Sagi, V. E. Clark, J. M. Platt, M. Kar, P. M. McCall, A. V. Zamudio, J. C. Manteiga, E. L. Coffey, C. H. Li, N. M. Hannett, et al., *Science* **2020**, *368*, 1386.
9. J. A. Riback, C. D. Katanski, J. L. Kear-Scott, E. V. Pilipenko, A. E. Rojek, T. R. Sosnick, D. A. Drummond, *Cell* **2017**, *168*, 1028.
10. W. Ma, C. Mayr, *Cell* **2018**, *175*, 1492.
11. W. Ma, G. Zheng, W. Xie, C. Mayr, *eLife* **2021**, *10*, 1.
12. X. Lin, Y. Qi, A. P. Latham, B. Zhang, *J. Chem. Phys.* **2021**, *155*, 010901.
13. A. G. Larson, D. Elnatan, M. M. Keenen, M. J. Trnka, J. B. Johnston, A. L. Burlingame, D. A. Agard, S. Redding, G. J. Narlikar, *Nature* **2017**, *547*, 236.
14. A. R. Strom, A. V. Emelyanov, M. Mir, D. V. Fyodorov, X. Darzacq, G. H. Karpen, *Nature* **2017**, *547*, 241.
15. B. R. Sabari, A. Dall'Agnese, E. Vasile, D. Hnisz, I. A. Klein, R. A. Young, J. C. Manteiga, S. Malik, T. I. Lee, B. J. Abraham, J. Schuijers, I. I. Cisse, R. G. Roeder, N. M. Hannett, D. S. Day, A. Boija, E. L. Coffey, K. Shrinivas, C. H. Li, P. A. Sharp, et al., *Science* **2018**, *361*, eaar3958.
16. W. Borcherds, A. Bremer, M. B. Borgia, T. Mittag, *Curr. Opin. Struct. Biol.* **2021**, *67*, 41.
17. A. A. Hyman, C. A. Weber, F. Jülicher, *Annu. Rev. Cell Dev. Biol.* **2014**, *30*, 39.
18. S. Boeynaems, S. Alberti, N. L. Fawzi, T. Mittag, M. Polymenidou, F. Rousseau, J. Schymkowitz, J. Shorter, B. Wolozin, L. Van Den Bosch, P. Tompa, M. Fuxreiter, *Trends Cell Biol.* **2018**, *28*, 420.
19. T. Mittag, R. V. Pappu, *Mol. Cell* **2022**, *82*, 2201.
20. G. L. Dignon, R. B. Best, J. Mittal, *Annu. Rev. Phys. Chem.* **2020**, *71*, 53.
21. S. F. Banani, A. M. Rice, W. B. Peeples, Y. Lin, S. Jain, R. Parker, M. K. Rosen, *Cell* **2016**, *166*, 651.
22. S. Ranganathan, E. I. Shakhnovich, *eLife* **2020**, *9*, e56159.
23. T. S. Harmon, A. S. Holehouse, M. K. Rosen, R. V. Pappu, *eLife* **2017**, *6*, 1.
24. H. Zhu, H. Fu, T. Cui, L. Ning, H. Shao, Y. Guo, Y. Ke, J. Zheng, H. Lin, X. Wu, G. Liu, J. He, X. Han, W. Li, X. Zhao, H. Lu, D. Wang, K. Hu, X. Shen, *Nucleic Acids Res.* **2022**, *50*, D340.
25. A. Jain, R. D. Vale, *Nature* **2017**, *546*, 243.

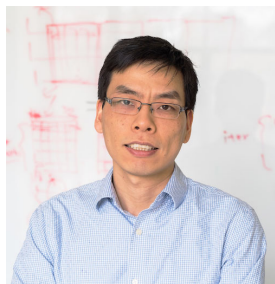
26. R. J. Ries, S. Zaccara, P. Klein, A. Olarerin-George, S. Namkoong, B. F. Pickering, D. P. Patil, H. Kwak, J. H. Lee, S. R. Jaffrey, *Nature* **2019**, *571*, 424.
27. E. M. Langdon, Y. Qiu, A. G. Niaki, G. A. McLaughlin, C. A. Weidmann, T. M. Gerbich, J. A. Smith, J. M. Crutchley, C. M. Termini, K. M. Weeks, S. Myong, A. S. Gladfelter, *Science* **2018**, *1*, 922.
28. M. Feric, N. Vaidya, T. S. Harmon, D. M. Mitrea, L. Zhu, T. M. Richardson, R. W. Kriwacki, R. V. Pappu, C. P. Brangwynne, *Cell* **2016**, *165*, 1686.
29. J. Fei, M. Jadalaha, T. S. Harmon, I. T. Li, B. Hua, Q. Hao, A. S. Holehouse, M. Reyer, Q. Sun, S. M. Freier, R. V. Pappu, K. V. Prasanth, T. Ha, *J. Cell Sci.* **2017**, *130*, 4180.
30. A. W. Folkmann, A. Putnam, C. F. Lee, G. Seydoux, *Science* **2021**, *373*, 1218.
31. S. Jain, J. R. Wheeler, R. W. Walters, A. Agrawal, A. Barsic, R. Parker, *Cell* **2016**, *164*, 487.
32. S. Elbaum-Garfinkle, Y. Kim, K. Szczepaniak, C. C. H. Chen, C. R. Eckmann, S. Myong, C. P. Brangwynne, *Proc. Natl. Acad. Sci. U.S.A.* **2015**, *112*, 7189.
33. J. Wang, J. M. Choi, A. S. Holehouse, H. O. Lee, X. Zhang, M. Jahnel, S. Maharana, R. Lemaitre, A. Pozniakovsky, D. Drechsel, I. Poser, R. V. Pappu, S. Alberti, A. A. Hyman, *Cell* **2018**, *174*, 688.
34. C. E. Sing, S. L. Perry, *Soft Matter* **2020**, *16*, 2885.
35. A. M. Rumyantsev, N. E. Jackson, J. J. De Pablo, *Annu. Rev. Condens. Matter Phys.* **2021**, *12*, 155.
36. P. R. Banerjee, A. N. Milin, M. M. Moosa, P. L. Onuchic, A. A. Deniz, *Angew. Chem.* **2017**, *129*, 11512.
37. J. E. Henninger, O. Oksuz, K. Shrinivas, I. Sagi, G. LeRoy, M. M. Zheng, J. O. Andrews, A. V. Zamudio, C. Lazaris, N. M. Hannett, T. I. Lee, P. A. Sharp, I. I. Cissé, A. K. Chakraborty, R. A. Young, *Cell* **2021**, *184*, 207.
38. F. Erdel, K. Rippe, *Biophys. J.* **2018**, *114*, 2262.
39. J. K. Ryu, C. Bouchoux, H. W. Liu, E. Kim, M. Minamino, R. de Groot, A. J. Katan, A. Bonato, D. Marenduzzo, D. Michieletto, F. Uhlmann, C. Dekker, *Sci. Adv.* **2021**, *7*.
40. C. P. Brangwynne, P. Tompa, R. V. Pappu, *Nat. Phys.* **2015**, *11*, 899.
41. C. M. Fare, A. Villani, L. E. Drake, J. Shorter, *Open Biol.* **2021**, *11*.
42. J. M. Choi, A. S. Holehouse, R. V. Pappu, *Annu. Rev. Biophys.* **2020**, *49*, 107.
43. L. Leibler, *Macromolecules* **1980**, *13*, 1602.
44. F. S. Bates, G. H. Fredrickson, *Annu. Rev. Phys. Chem.* **1990**, *41*, 525.
45. S. F. Shimobayashi, P. Ronceray, D. W. Sanders, M. P. Haataja, C. P. Brangwynne, *Nature* **2021**, *3*.
46. B. Gouveia, Y. Kim, J. W. Shaevitz, S. Petry, H. A. Stone, C. P. Brangwynne, *Nature* **2022**, *609*, 255.
47. H. Tschochner, E. Hurt, *Trends Cell Biol.* **2003**, *13*, 255.
48. F. M. Boisvert, S. Van Koningsbruggen, J. Navascués, A. I. Lamond, *Nat. Rev. Mol. Cell Biol.* **2007**, *8*, 574.
49. D. L. Lafontaine, J. A. Riback, R. Bascetin, C. P. Brangwynne, *Nat. Rev. Mol. Cell Biol.* **2021**, *22*, 165.
50. K. A. Alexander, A. Coté, S. C. Nguyen, L. Zhang, O. Ghulamalamdari, P. Agudelo-Garcia, E. Lin-Shiao, K. M. Tanim, J. Lim, N. Biddle, M. C. Dunagin, C. R. Good, M. R. Mendoza, S. C. Little, A. Belmont, E. F. Joyce, A. Raj, S. L. Berger, *Mol. Cell* **2021**, *81*, 1666.
51. S. Xu, S.-K. Lai, D. Y. Sim, W. Ang, H. Y. Li, X. Roca, *Nucleic Acids Res.* **2022**, *50*, 8599.
52. I. A. Ilik, M. Malszycki, A. K. Lübke, C. Schade, D. Meierhofer, T. Aktas, *eLife* **2020**, *9*, 1.
53. S. E. Liao, O. Regev, *Nucleic Acids Res.* **2021**, *49*, 636.
54. C. P. Brangwynne, C. R. Eckmann, D. S. Courson, A. Rybarska, C. Hoege, J. Gharakhani, F. Julicher, A. A. Hyman, *Science* **2009**, *324*, 1729.
55. J. Smith, D. Calidas, H. Schmidt, T. Lu, D. Rasoloson, G. Seydoux, *eLife* **2016**, *5*, 1.
56. A. Putnam, M. Cassani, J. Smith, G. Seydoux, *Nat. Struct. Mol. Biol.* **2019**, *26*.
57. T. Lu, E. Spruijt, *J. Am. Chem. Soc.* **2020**, *142*, 2905.
58. S. Hoffmann, N. Kedersha, P. Anderson, P. Ivanov, *Biochim. Biophys. Acta Mol. Cell Res.* **2021**, *1868*, 118876.
59. B. Niewidok, M. Igaev, A. P. da Graca, A. Strassner, C. Lenzen, C. P. Richter, J. Piehler, R. Kurre, R. Brandt, *J. Cell Biol.* **2018**, *217*, 1303.
60. J. R. Wheeler, T. Matheny, S. Jain, R. Abrisch, R. Parker, *eLife* **2016**, *5*, 1.
61. S. Choi, M. C. Meyer, P. C. Bevilacqua, C. D. Keating, *Nat. Chem.* **2022**, *14*.
62. J. A. West, M. Mito, S. Kurosaka, T. Takumi, C. Tanegashima, T. Chujo, K. Yanaka, R. E. Kingston, T. Hirose, C. Bond, A. Fox, S. Nakagawa, *J. Cell Biol.* **2016**, *214*, 1.
63. H. Yu, S. Lu, K. Gasior, D. Singh, S. Vazquez-Sanchez, O. Tapia, D. Toprani, M. S. Beccari, J. R. Yates, S. Da Cruz, J. M. Newby, M. Lafarga, A. S. Gladfelter, E. Villa, D. W. Cleveland, *Science* **2021**, *371*.
64. J. G. Gall, M. Bellini, Z. Wu, C. Murphy, *Mol. Biol. Cell* **1999**, *10*, 4385.
65. H. Suzuki, R. Abe, M. Shimada, T. Hirose, H. Hirose, K. Noguchi, Y. Ike, N. Yasui, K. Furugori, Y. Yamaguchi, A. Toyoda, Y. Suzuki, T. Yamamoto, N. Saitoh, S. Sato, C. Tomomori-Sato, R. C. Conaway, J. W. Conaway, H. Takahashi, *Nat. Commun.* **2022**, *13*, 2905.
66. M. Feric, A. Sarfallah, F. Dar, D. Temiakov, R. V. Pappu, T. Misteli, *Proc. Natl. Acad. Sci. U.S.A.* **2022**, *119*, e2207303119.
67. M. Feric, T. G. Demarest, J. Tian, D. L. Croteau, V. A. Bohr, T. Misteli, *EMBO J.* **2021**, *40*, e107165.
68. Y. Shin, C. P. Brangwynne, *Science* **2017**, *357*.
69. G. A. Mountain, C. D. Keating, *Biomacromolecules* **2020**, *21*, 630.
70. P. J. Flory, *J. Chem. Phys.* **1942**, *10*, 51.
71. E. Helfand, Y. Tagami, *J. Chem. Phys.* **1972**, *56*, 3592.
72. R. J. Roe, *J. Chem. Phys.* **1975**, *62*, 490.
73. S. Boeynaems, A. S. Holehouse, V. Weinhardt, D. Kovacs, J. Van Lindt, C. Larabell, L. V. D. Bosch, R. Das, P. S. Tompa, R. V. Pappu, A. D. Gitler, *Proc. Natl. Acad. Sci. U.S.A.* **2019**, *116*, 7889.
74. R. S. Fisher, S. Elbaum-Garfinkle, *Nat. Commun.* **2020**, *11*.
75. J. R. Simon, N. J. Carroll, M. Rubinstein, A. Chilkoti, G. P. López, *Nat. Chem.* **2017**, *9*, 509.
76. A. P. Latham, B. Zhang, *Biophys. J.* **2022**, *121*, 1727.
77. R. M. Regy, G. L. Dignon, W. Zheng, Y. C. Kim, J. Mittal, *Nucleic Acids Res.* **2020**, *48*, 12593.
78. T. S. Harmon, A. S. Holehouse, R. V. Pappu, *New J. Phys.* **2018**, *20*.
79. I. Sanchez-Burgos, J. R. Espinosa, J. A. Joseph, R. Collepardo-Guevara, *Biomolecules* **2021**, *11*, 1.
80. A. P. Latham, B. Zhang, *J. Chem. Theory Comput.* **2020**, *16*, 773–781.

81. A. P. Latham, B. Zhang, *J. Chem. Theory Comput.* **2021**, *17*, 3134.
82. A. P. Latham, B. Zhang, *Curr. Opin. Struct. Biol.* **2022**, *72*, 63.
83. R. Leicher, A. Osunsade, G. N. L. Chua, S. C. Faulkner, A. P. Latham, J. W. Watters, T. Nguyen, E. C. Beckwitt, S. Christodoulou-rubalcava, P. G. Young, B. Zhang, Y. David, S. Liu, *Nat. Struct. Mol. Biol.* **2022**, *29*, 463.
84. T. Pal, J. Wessén, S. Das, H. S. Chan, *Phys. Rev. E* **2021**, *103*, 042406.
85. A. S. Holehouse, G. M. Ginell, D. Griffith, E. Böke, *Biochemistry* **2021**.
86. A. Patel, H. O. Lee, L. Jawerth, S. Maharana, M. Jahnel, M. Y. Hein, S. Stoyanov, J. Mahamid, S. Saha, T. M. Franzmann, A. Pozniakovski, I. Poser, N. Maghelli, L. A. Royer, M. Weigert, E. W. Myers, S. Grill, D. Drechsel, A. A. Hyman, S. Alberti, *Cell* **2015**, *162*, 1066.
87. A. Garaizar, J. R. Espinosa, J. A. Joseph, R. Collepardo-Guevara, *Sci. Rep.* **2022**, *12*, 4390.
88. T. Kaur, M. Raju, I. Alshareedah, R. B. Davis, D. A. Potoyan, P. R. Banerjee, *Nat. Commun.* **2021**, *12*.
89. A. G. Pyo, Y. Zhang, N. S. Wingreen, *iScience* **2022**, *25*, 103852.
90. Y. Qi, A. Reyes, S. E. Johnstone, M. J. Aryee, B. E. Bernstein, B. Zhang, *Biophys. J.* **2020**, pp. 1–28.
91. K. Kamat, Y. Qi, Y. Wang, J. Ma, B. Zhang, *bioRxiv* **2021**, p. 2021.11.12.468401.
92. Z. Jiang, B. Zhang, *Phys. Rev. Lett.* **2019**, *123*, 208102.
93. Z. Jiang, B. Zhang, *PLOS Comput. Biol.* **2021**, *17*, e1008556.
94. Z. Jiang, Y. Qi, K. Kamat, B. Zhang, *J. Phys. Chem. B* **2022**.
95. D. Kashchiev, *Nucleation*, Elsevier **2000**.
96. A. McGaughey, C. Ward, *J. Appl. Phys.* **2003**, *93*, 3619.
97. C. P. Brangwynne, T. J. Mitchison, A. A. Hyman, *Proc. Natl. Acad. Sci. U.S.A.* **2011**, *108*, 4334.
98. M. Grosch, S. Ittermann, D. Shaposhnikov, M. Drukker, *Stem Cell Rep.* **2020**.
99. D. L. Spector, A. I. Lamond, *Cold Spring Harb. Perspect. Biol.* **2011**, *3*, a000646.
100. I. Sanchez-Burgos, J. A. Joseph, R. Collepardo-Guevara, J. R. Espinosa, *Sci. Rep.* **2021**, *11*, 1.
101. M. Garcia-Jove Navarro, S. Kashida, R. Chouaib, S. Souquere, G. Pierron, D. Weil, Z. Gueroui, *Nat. Commun.* **2019**, *10*, 1.
102. Y. Qi, B. Zhang, *Nat. Commun.* **2021**, p. 6824.
103. D. W. Sanders, N. Kedersha, D. S. Lee, A. R. Strom, V. Drake, J. A. Riback, D. Bracha, J. M. Eeftens, A. Iwanicki, A. Wang, M. T. Wei, G. Whitney, S. M. Lyons, P. Anderson, W. M. Jacobs, P. Ivanov, C. P. Brangwynne, *Cell* **2020**, *181*, 306.
104. P. Yang, C. Mathieu, R. M. Kolaitis, P. Zhang, J. Messing, U. Yurtsever, Z. Yang, J. Wu, Y. Li, Q. Pan, J. Yu, W. Erik, T. Mittag, H. J. Kim, J. P. Taylor, *Cell* **2021**, *181*, 325.
105. Y. Yang, Z. Fang, X. Chen, W. Zhang, Y. Xie, Y. Chen, Z. Liu, W. Yuan, *Front. Pharmacol.* **2017**, *8*, 1.
106. T. J. Welsh, G. Krainer, J. R. Espinosa, J. A. Joseph, A. Sridhar, M. Jahnel, W. E. Arter, K. L. Saar, S. Alberti, R. Collepardo-Guevara, T. P. Knowles, *Nano Lett.* **2022**, *22*, 612.
107. C. P. Brangwynne, T. J. Mitchison, A. A. Hyman, *Proc. Natl. Acad. Sci. U.S.A.* **2011**, *108*, 4334.
108. Y. Zhang, D. S. Lee, Y. Meir, C. P. Brangwynne, N. S. Wingreen, *Phys. Rev. Lett.* **2021**, *126*, 258102.
109. R. W. Style, T. Sai, N. Fanelli, M. Ijavi, K. Smith-Mannschott, Q. Xu, L. A. Wilen, E. R. Dufresne, *Phys. Rev. X* **2018**, *8*, 11028.
110. K. A. Rosowski, T. Sai, E. Vidal-Henriquez, D. Zwicker, R. W. Style, E. R. Dufresne, *Nat. Phys.* **2020**, *16*, 422.
111. D. S. Lee, N. S. Wingreen, C. P. Brangwynne, *Nat. Phys.* **2021**, *17*, 531.
112. A. Zidovska, *Cell* **2020**, *183*, 1737.
113. J. D. Wurtz, C. F. Lee, *Phys. Rev. Lett.* **2018**, *120*, 78102.
114. J. Söding, D. Zwicker, S. Sohrabi-Jahromi, M. Boehning, J. Kirschbaum, *Trends Cell Biol.* **2020**, *30*, 4.
115. B. Guilhas, J. C. Walter, J. Rech, G. David, N. O. Walliser, J. Palmeri, C. Mathieu-Demaziere, A. Parmeggiani, J. Y. Bouet, A. Le Gall, M. Nollmann, *Mol. Cell* **2020**, *79*, 293.
116. J. T. Wang, J. Smith, B. C. Chen, H. Schmidt, D. Rasoloson, A. Paix, B. G. Lambrus, D. Calidas, E. Betzig, G. Seydoux, *eLife* **2014**, *3*, 1.
117. J. D. Wurtz, C. F. Lee, *New J. Phys.* **2018**, *20*.
118. F. Wippich, B. Bodenmiller, M. G. Trajkovska, S. Wanka, R. Aebersold, L. Pelkmans, *Cell* **2013**, *152*, 791.

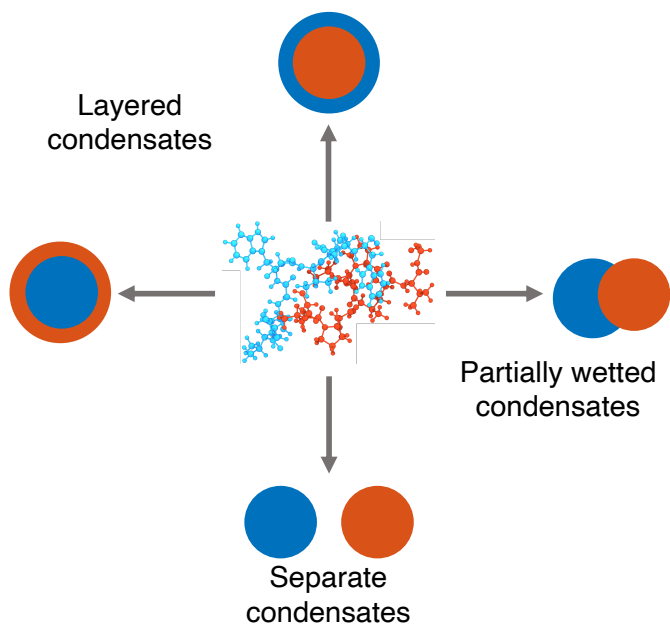
## AUTHOR BIOGRAPHIES



**Andrew P. Latham** received his B.S. from the University of Notre Dame. He completed a Ph.D. in Chemistry from the Massachusetts Institute of Technology under the supervision of Dr. Bin Zhang in May 2022, and is now a postdoctoral scholar in Andrej Sali's group at the University of California, San Francisco. His research interests focus on leveraging existing experimental data to build high resolution computational models of complex biological systems, including membraneless organelles.



**Bin Zhang** obtained his Ph.D. from the California Institute of Technology, where he worked with Thomas F. Miller on Sec-facilitated protein translocation and membrane integration. Upon graduation, Bin accepted a position as a postdoctoral scholar with Peter G. Wolynes at the Center for Theoretical Biological Physics at Rice University. He joined Massachusetts Institute of Technology in 2016, where he is the Pfizer-Laubach Career Development Associate Professor of Chemistry. His group develops multiscale coarse-graining approaches to simulate the organization of biocondensates and the human genome.



Abstract Figure

